STRUCTURAL, DIELECTRIC AND PYROELECTRIC PROPERTIES OF Nb AND Fe DOPED PZT CERAMICS

V. STANCU[a], L. AMARANDE[a], M. BOTEA[a], M. CIOANGHER[a],
A.G. TOMULESCU[b], A. IUGA[a], L. PINTILIE[a*]
[a]*National Institute of Materials Physics, Atomistilor Str., No. 405A, 077125, Magurele-Ilfov Romania*
[b]*University of Bucharest, Faculty of Physics, 077125 Magurele Romania*

Lead zirconate titanate doped with iron and niobium (PZFNT) was prepared by conventional processing technique, solid state synthesis method. The influence of dopants on the microstructure, ferroelectric and pyroelectric properties was investigated. XRD data reveals a perovskite structure near to the lead zirconate phase. The relative density of PZFNT is approximate 90%, with average grains size of 6.45µm.

1. Introduction

Lead zirconate titanate $Pb(Zr_xTi_{1-x})O_3$ (PZT) as bulk ceramic or thin film has been extensively studied due to ferroelectric, pyroelectric and piezoelectric properties and it is used in many application [1,2]. As bulk ceramics, PZT is a good material for microelectronics industry. In order to obtain the desired properties PZT ceramics are doped with small amounts of other oxide materials, most popular are oxide based on lanthanum and niobium [3-5]. This combination of doped PZT was investigated as films [6,7] but more studies were made on bulk ceramics [8-10].

In this study was investigated the role of a new combination of dopants, an old one - niobium, combined with a new one - iron, with respect to the structural and pyroelectric properties.

2. Experimental

Lead zirconate titanate ceramic doped with iron and, niobium ($PbZr_{0.68}Fe_{0.14}Nb_{0.14}Ti_{0.04}O_3$, PZFNT) was prepared by the solid state synthesis method. The starting reagents for PZFNT were lead oxide PbO (Merck, 99.7%), zirconium oxide ZrO_2 (Fluka, 99.8%), niobium pentoxide Nb_2O_5 (Fluka, 99.7%), iron trioxide Fe_2O_3 (Merck, 99.8%) and titanium dioxide TiO_2 (Fluka, 99.5%). PZFNT was prepared with 1.5% (molar percent) excess lead oxide to compensate the deficiency in lead concentration and to assist the crystallization. Ethanol (Chimopar, 99.6%) was used as solvent. The ceramics were prepared according to the procedure presented in Fig. 1.
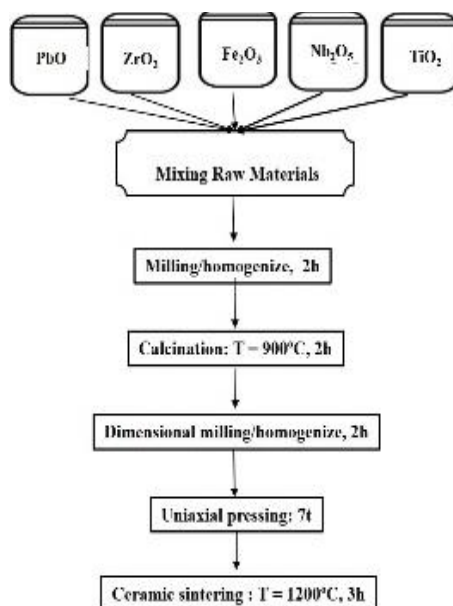
---

* Corresponding author: pintilie@infim.ro

226

Fig 1. Flow diagram for the solid state processing of PZFNT ceramics.

Raw materials were mechanically mixed in a RETSCH planetary ball mill for good homogenization at 300 rpm for 2 hours. In order to eliminate the solvent, the PZFNT powder was dried at 150°C followed by calcination at 900°C for 2 hours. The PZFNT ceramic pellets with 30 mm diameter were obtained by cold pressing, while applying an equivalent force of 7 tones. These structures were sintered at 1200°C for 3 hours (2°C/min heating rate). In this way, compact ceramics with 7.11g/cm^3 density were obtained.

PZFNT ceramics microstructure was studied by using a Tesca Lyra 3XMU scanning electron microscope (SEM). The crystal structure was analyzed by X-ray Diffraction (XRD) using a *Bruker D8 Advance* equipment (powder setting). For electrical characterization 200 µm thick Ni/Ag electrodes were deposited on both faces of PZFNT pallets with 30 mm diameter.

The hysteresis measurements were performed with a Precision LC II ferroelectric tester from Radiant Technologies Inc. The temperature dependent measurements were performed by placing the sample in a cryostat from Janis Research, allowing temperature variation from liquid N_2 to about 450 K. The capacitance was measured with a Hioki LCR bridge, while the charge was recorded with the aid of a Keithley picoammeter. The pyroelectric signal was recorded with a SR 830 DSP lock-in amplifier, using an J-FET type impedance converter (sample placed on the gate contact, a dc voltage of 7 V applied on the drain contact, and signal collected from a 100 kΩ resistance placed between source contact and ground). The IR source was a laser diode of 40 mW at 800 nm. The beam was modulated electronically using a signal generator from Tektronix, model AFG 3052C.

3. Results and discussion

The morfology of PZFNT displays a good compactation structure of ceramics with small pores between grains, with an average grain size of 6.45 µm (see Fig. 2). Large grains and relatively low densities are correlated with the decreased diffusivity of lead [11]

The crystalline structure of PZFNT ceramics analyzed by XRD was revealed through sharp and intense peaks corresponding solely to orthorhombic phase, indexed according to ASTM pattern 35-0739 (figure 3). The presence of Nb^{5+} can induce the fluorite phase [12] in the case of thin films, but in our bulk ceramics secondary phase is not observed.
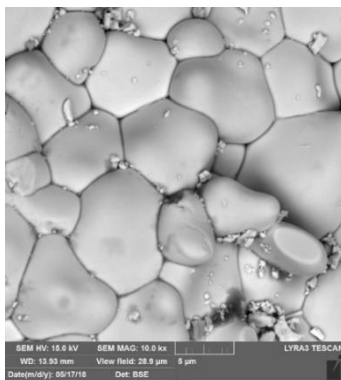
Fig 2. The SEM images of the fractured PZFNT ceramic.

The addition of dopants substituting the B- site (Nb^{5+} and Fe^{3+} substitute Zr/Ti positions) can cause changes in the lattice parameters. After indexing the XRD powder pattern (Fig. 3) we calculated the lattice constants of PZNFT ceramic: a = 8.2519Å, b = 11.7242 Å, c = 5.8281 Å. Considering the PZT phase diagram that supports the formation of an orthorhombic phase and the ASTM pattern 35-0739, we can observe a lattice distortion consisting in an elongated *a* parameter and decreased *b* and *c* parameters.
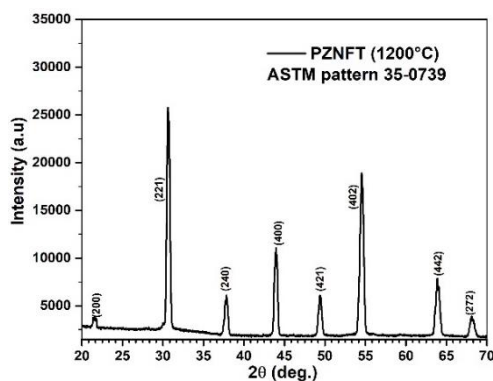

Fig 3. XRD pattern of PZFNT ceramics.

The result of hysteresis measurement is presented in Fig. 4. The loop is almost rectangular and saturated at electric fields not exceeding 40 kV/cm. The remnant polarization is around 16 $\mu C/cm^2$ while the coercive field 8 kV/cm.
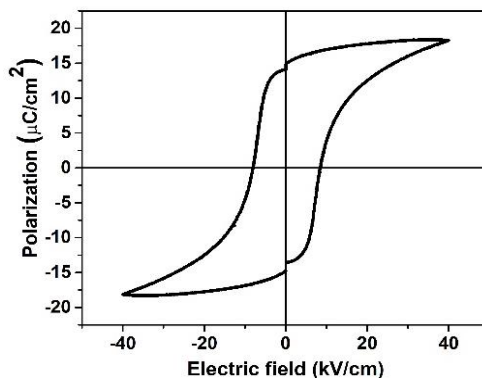

Fig 4. Polarization hysteresis loops for PZNFT samples.

Therefore, the sample was poled with 40 kV/cm, then placed in a cryostat and cooled down to about -155 °C. The charge variation during heating up the sample at a constant rate of 3 K/min was recorded. This should be the same with the polarization variation between the starting and ending temperature, thus between about -155 °C and +185 °C. The result is presented in Fig. 5a. One has to underline that the cryostat does not allow heating above the transition temperature, thus the zero in Fig. 5a does not mean that the polarization has vanished, it is only to help visualizing the polarization variation during the measurement. The polarization variation with temperature was then used to extract the value of the pyroelectric coefficient on the same temperature range, knowing that pyroelectric coefficient $p = dP/dT$, where P is polarization and T temperature. The result is presented in Fig. 5b.
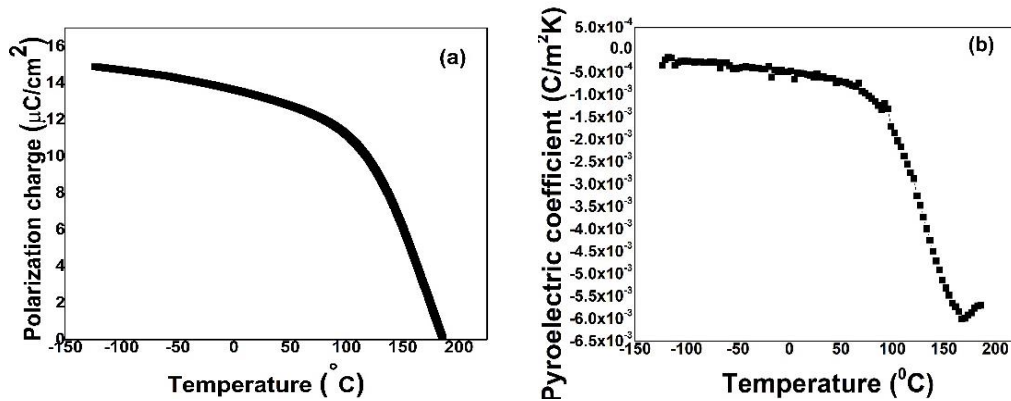

Fig 5. Polarization vs. temperature (a) and pyroelectric coefficient vs temperature (b) for the PZNFT pellets.

One can notice that the pyroelectric coefficient around room temperature (25 °C) is about 6×10^{-4} C/m^2K. This value is comparable or even larger than previous reports in literature for PZT ceramics with similar doping elements [13-15]. The dielectric constant and dielectric losses were also estimated from capacitance measurements performed in the same temperature range in order to extract information on the pyroelectric figure of merit (see graphs in Fig. 6). The values around room temperature are of about 180 for dielectric constant, and about 2.6 % for dielectric losses.
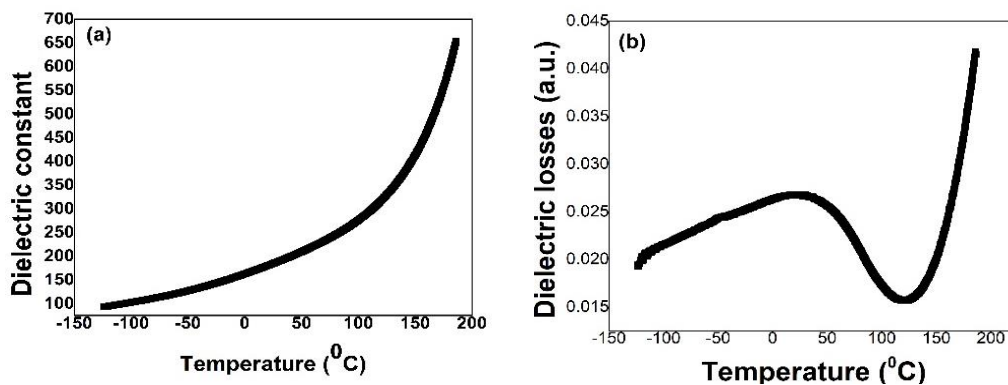

Fig 6. The influence of temperature on dielectric constant (a) and dielectric losses (b) for PZNFT ceramic.

Being designated to work in the pyroelectric voltage mode, the most suitable figures of merit to compare the present results with previous reports in literature are F_v and F_D, defined by the following relations [16]:

$$F_v = p'/c'\,\varepsilon\varepsilon_o$$

$$F_D = p'/c'\,(\varepsilon\varepsilon_o\,\tan\delta)^{1/2}$$

Here p' is the pyroelectric coefficient, c' is the volume specific heat, ε is the dielectric constant, ε_0 is the vacuum permittivity and $\tan\delta$ are the dielectric losses. A value of 2.6×10^6 J/m^3 K was considered for c' [17]. Using the values presented above for p', ε and $\tan\delta$, the following values are obtained for the two figures of merit at room temperature: $F_v = 0.144$ m^2/C and $F_D = 3.58\times10^{-5}$ Pa$^{1/2}$. The value of F_v is larger than previous reports [13, 18], while the value of F_d is comparable and can be enhanced by reducing the dielectric losses.
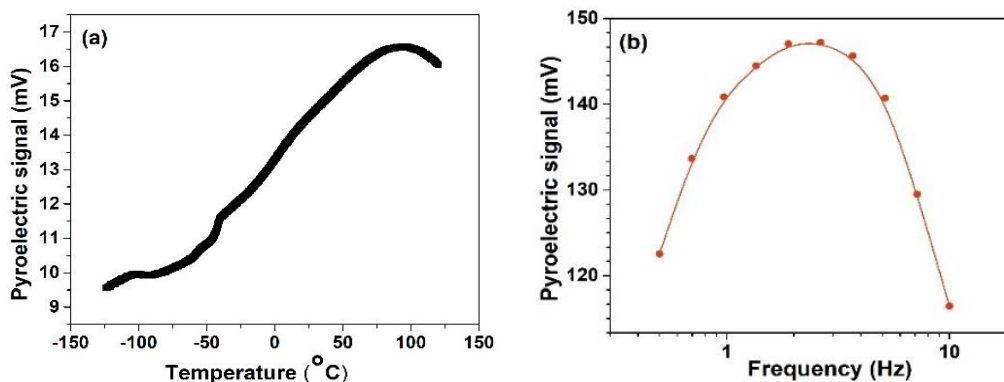

Fig 7. Pyroelectric signal vs. temperature (a) and frequency (b) for the PZNFT ceramic.

The Fe and Nb doped PZT ceramic was then used as an active element in a pyroelectric detector working in the voltage mode. The temperature and frequency dependencies of the measured pyroelectric signal are presented in Fig. 7. A robust signal can be measured on a wide temperature domain providing that the modulation frequency of the incident IR beam is around 3 Hz (maximum observed in the frequency dependence).

4. Conclusions

In conclusion, in this work we have reported the effect of Fe and Nb on structural, electrical and pyroelectric properties of PZT ceramics. Morfo - structural studies confirm perovskite phase, good homogeneity and crystallization of the ceramics. The obtained pyroelectric coefficient is about 6×10^{-4} C/m^{2}K, good value to produced ceramics with suitable properties to be employed in sensing devices such as pyroelectric detectors for infrared radiation.

References

[1] J. F. Scott, Advanced Microelectronics Series (Ed), Ferroelectric Memories, Springer–Verlag Berlin Heidelberg, 2000.
[2] A. C. Galca, V. Stancu, M. A. Husanu et al., Applied Surface Science **257**, 5938 (2011).
[3] Volkan Kalem, Ibrahim C¸ Muharrem Timuc¸ Ceramics International **37**, 1265 (2011).
[4] H. Goudarzi, S. Baghshahi, Ceramics International **43**, 3873 (2017).

230

[5] Heng Chang Nie, Xian Lin Dong, Ning Bo Feng, et al, Materials Research Bulletin **45**, 564 (2010).

[6] L. Pintilie, I. Boerasu, M. Pereira, M.J.M. Gomes, Materials Science and Engineering B **109**(1-3), 174 (2004).

[7] W. Bai, X. J. Meng, T. Lin, et al, Journal of Applied Physics **106**, 124908 (2009).

[8] Junxia Wang, Genshui Wang, Jin Wang, Xuefeng Chen et al., Ceramics International **l42**, 10105 (2016).

[9] A. Hizebry, H. El Attaoui, M. Saadaoui et al., Journal of the European Ceramic Society **27**, 557 (2007).

[10] M. Cerqueira, R. S. Nasar, E. Longo et al., Journal Of Materials Science **32**, 2381 (1997).

[11] A. Kumar, S. K. Mishra, Adv. Matter Lett. **5**(8), 479 (2014).

[12] L. Pintilie, M. Pereira, M. J. M. Gomes, I. Boerasu, Sensors and Actuators A **115**, 185 (2004).

[13] Farhad Fouladi, Ehsan Javid, Yousef Seyed Jalili, J. Mater Sci: Mater Electron **27**, 6578 (2016).

[14] K. W. Kwok, R. C. W. Tsang, H. L. W. Chan, C. L. Choy, J Sol-Gel Sci. Technol. **47**, 148 (2008).

[15] O. P. Thakur, J. P. Singh, C. Prakash, P. Kishan, Defence Science Journal **57**(3), 233 (2007).

[16] R. W. Whatmore, Rep. Prog. Phys. **49**, 1335 (1986).

[17] M. Botea, A. Iuga, L. Pintilie, Applied Physics Letters **103**, 232902 (2013).

[18] R.W. Whatmore, Journal of Electroceramics **13**, 139 (2004).